# Strongly Correlated Materials from a Numerical Renormalization Group Perspective: How the Fermi-Liquid State of $Sr_2RuO_4$ Emerges

Fabian B. Kugler,[1] Manuel Zingl,[2] Hugo U. R. Strand,[2] Seung-Sup B. Lee,[1] Jan von Delft,[1] and Antoine Georges[3,2,4,5]

[1]*Arnold Sommerfeld Center for Theoretical Physics, Center for NanoScience, and Munich Center for Quantum Science and Technology, Ludwig-Maximilians-Universität München, 80333 Munich, Germany*

[2]*Center for Computational Quantum Physics, Flatiron Institute, 162 5th Avenue, New York, New York 10010, USA*

[3]*Collège de France, 11 place Marcelin Berthelot, 75005 Paris, France*

[4]*Centre de Physique Théorique, CNRS, Ecole Polytechnique, IP Paris, 91128 Palaiseau, France*

[5]*Department of Quantum Matter Physics, University of Geneva, 1211 Geneva 4, Switzerland*

(Received 5 September 2019; published 2 January 2020)

The crossover from fluctuating atomic constituents to a collective state as one lowers temperature or energy is at the heart of the dynamical mean-field theory description of the solid state. We demonstrate that the numerical renormalization group is a viable tool to monitor this crossover in a real-materials setting. The renormalization group flow from high to arbitrarily small energy scales clearly reveals the emergence of the Fermi-liquid state of $Sr_2RuO_4$. We find a two-stage screening process, where orbital fluctuations are screened at much higher energies than spin fluctuations, and Fermi-liquid behavior, concomitant with spin coherence, below a temperature of 25 K. By computing real-frequency correlation functions, we directly observe this spin-orbital scale separation and show that the van Hove singularity drives strong orbital differentiation. We extract quasiparticle interaction parameters from the low-energy spectrum and find an effective attraction in the spin-triplet sector.

DOI: 10.1103/PhysRevLett.124.016401

*Introduction.*—Atoms with partially filled shells have a spectrum of many-body eigenstates with degeneracies associated with fluctuating spin and orbital moments. For instance, the isolated ruthenium atom in the $Ru^{4+}$ configuration, subject to an octahedral crystal field, has a ninefold degenerate ground state corresponding to spin and orbital quantum numbers $S = L = 1$ [1,2]. In materials with strong electronic correlations, these local fluctuations can be observed at high temperature and energy through, e.g., Curie–Weiss-like spin susceptibilities. In correlated metals, these fluctuations are suppressed as one reaches low temperature and energy. In the Fermi-liquid regime, a nondegenerate collective ground state is formed, with long-lived coherent quasiparticle excitations and susceptibilities displaying Pauli behavior [3].

How the crossover from fluctuating atomic constituents to a collective state takes place is at the heart of the dynamical mean-field theory (DMFT) description of the solid state [4]. In this theory, each atom is viewed as exchanging electrons with an environment which self-consistently represents the whole solid. The gradual suppression of local fluctuations can be thought of as a self-consistent (multistage) Kondo screening process [5] of both spin and orbital moments [6,7].

The renormalization group (RG) is the appropriate framework to describe and monitor these crossovers as a function of energy scale. Indeed, Wilson's numerical renormalization group (NRG) [8] has been a tool of choice for solving DMFT equations for lattice models with few orbital degrees of freedom [9], with the additional merit of providing real-frequency properties at any temperature. Following a number of two-particle applications [10–15], recently, even three-orbital studies have become possible [6,7,16–19]. Yet, all of these works operated in the model context. We demonstrate here that NRG can be successfully applied to an actual material, accounting for its electronic structure in a realistic manner using density functional theory (DFT) and DMFT [20].

The material we focus on, $Sr_2RuO_4$, is one of the more thoroughly studied quantum materials [21] and an ideal test bed for fundamental developments in quantum many-body theories. Besides the unconventional superconducting state below $\sim$1.5 K [22,23], also the normal, Hund-metal state of $Sr_2RuO_4$ [2,7,24–27] attracts attention, due to textbook Fermi-liquid behavior below $T_{\mathrm{FL}} \approx 25$ K [21,28–33] (though signatures of quasiparticles are found up to elevated temperatures of $\sim$600 K [24]). However, temperatures below $T_{\mathrm{FL}}$ could not be reached with controlled computational methods hitherto.

In this Letter, we show that $Sr_2RuO_4$ undergoes a two-stage Kondo screening process [6,7,26], where orbital fluctuations are screened well before the spin degrees of freedom. We determine the associated Kondo temperatures to $T_{\mathrm{orb}} \approx 6000$ K and $T_{\mathrm{sp}} \approx 500$ K, respectively, and show

 

that Fermi-liquid behavior emerges when spin coherence is *fully* established below a scale of $T_{\mathrm{FL}} \approx 25$ K [34]. With NRG as impurity solver, the entire DMFT calculation is performed on the real-frequency axis [35], and we can compute correlation functions at arbitrarily low energy scales and temperatures. Hence, we are able to go beyond previous Monte Carlo–based DFT + DMFT studies [24,26,27,33,38–41] and enter deep into the Fermi-liquid regime, even down to $T = 0$ [42]. This enables us to explore the counterintuitive observation that the more itinerant ($xy$) orbital has the smaller quasiparticle weight [21,24,27,38,41,44,45]. We show that this effect is driven by a van Hove singularity close to the Fermi level, as elaborated in Ref. [24].

*Model.*—The low-energy structure of $Sr_2RuO_4$ can be well described by a local basis of three maximally localized Wannier functions [46,47] with Ru-4d $t_{2g}$ symmetry denoted by $\{xy, xz, yz\}$. The corresponding noninteracting Wannier Hamiltonian is characterized by the density of states (DOS) shown in Fig. 3(a) below, reflecting the quasi-2D tetragonal crystal structure of $Sr_2RuO_4$, with quasi-2D $xy$ orbitals and a strongly one-dimensional character of the degenerate $xz/yz$ orbitals. We employ the same Wannier Hamiltonian as in Refs. [39,40,48] (without spin-orbit coupling) combined with a local Kanamori interaction [2,49], $H_{\mathrm{int}} = (U - 3J)N(N-1)/2 - 2J\boldsymbol{S}^2 - J\boldsymbol{L}^2/2$, parametrized by $U = 2.3$ and $J = 0.4$ [24]. Throughout this work, we use eV $= 1$ as the unit of energy if not otherwise indicated. In the Hund-metal phase of $Sr_2RuO_4$, the pair-hopping term of the Kanamori interaction, as part of $-J\boldsymbol{L}^2/2$, is almost inactive. It can thus be neglected to obtain a model with higher symmetry, which is more tractable for NRG, as explained in Ref. [50].

*Spin-orbital separation, Fermi liquid.*—Since NRG can reach arbitrarily small energy scales, we are able to directly observe both spin-orbital scale separation and the onset of Fermi-liquid behavior. The zero-temperature real-frequency orbital and spin susceptibilities [50], $\chi''_{\mathrm{orb}}$ and $\chi''_{\mathrm{sp}}$, exhibit a separation of their maxima by more than one decade, see Fig. 1(a). This spin-orbital separation in Kondo scales, with $T_{\mathrm{orb}} \approx 6000$ K and $T_{\mathrm{sp}} \approx 500$ K as found from the maxima of $\chi''$, is distinctive of correlated Hund metals [2,6,7,19], where the Hund coupling $J$ causes the screening of the respective fluctuations to occur at disparate energy scales. Further, the *completed* screening of fluctuations [7] is signaled by linear behavior, $\chi'' \propto \omega$, found below roughly 1000 K and 25 K for $\chi''_{\mathrm{orb}}$ and $\chi''_{\mathrm{sp}}$, respectively. The fully coherent Fermi-liquid state thus emerges below an energy scale of 25 K. The Fermi-liquid onset is also seen in the temperature dependence of the static spin susceptibility, $\chi_{\mathrm{sp}}(\omega = 0)$, which crosses over from Curie–Weiss- to Pauli-like behavior, saturating below $T_{\mathrm{FL}} \approx 25$ K, see inset of Fig. 1(a). These results clearly establish spin-orbital scale separation in the low-temperature Fermi-liquid state of $Sr_2RuO_4$, as proposed by previous studies above $T_{\mathrm{FL}}$ [7,26].

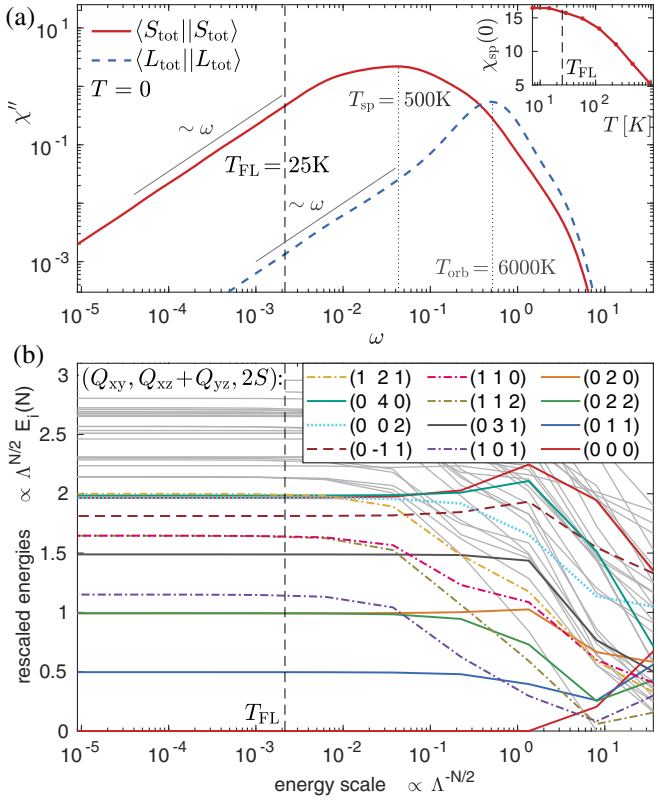


FIG. 1. (a) Dynamic spin and orbital susceptibilities, $\chi''_{\mathrm{sp}}(\omega)$ and $\chi''_{\mathrm{orb}}(\omega)$, showing spin-orbital scale separation. Inset: Static spin susceptibility as a function of temperature. (b) NRG flow diagram, showing the rescaled eigenenergies (with quantum numbers given in the legend) as a function of the energy scale [50], for the impurity model at self-consistency. The spin and orbital Kondo temperatures (maximum of $\chi''$) and the Fermi-liquid scale, $T_{\mathrm{FL}}$, are marked by vertical lines.

A very direct observation of Fermi-liquid behavior is possible by studying the renormalization group flow diagram of the NRG algorithm [6,9,18,19]. Figure 1(b) shows the NRG Hamiltonian's (lowest) rescaled eigenenergies, $\Lambda^{N/2}E_i(N)$, depending on the energy scale $\Lambda^{-N/2}$ of the RG flow, where $\Lambda$ is the NRG discretization parameter and $N$ the length of the Wilson chain [50]. At high energy, the states are pure atomic eigenstates, which are screened by the bath when flowing down in energy. Below $T_{\mathrm{FL}}$, the Fermi liquid is formed. There, the flow reaches a fixed point, where the rescaled eigenenergies become independent of $N$, $\Lambda^{N/2}E_i(N) = E_i^*$. The Fermi-liquid nature of this fixed point is determined by "towers" [9] of equidistant excitation energies within the same symmetry sector, where each $E_i^*$ is composed of $n$ quasiparticle excitations, $E_i^* = nE_{\mathrm{qp}}$.

Each eigenstate has the quantum numbers $(Q_{xy}, Q_{xz}+Q_{yz}, 2S)$, with orbital-resolved charge $Q_m$ relative to the

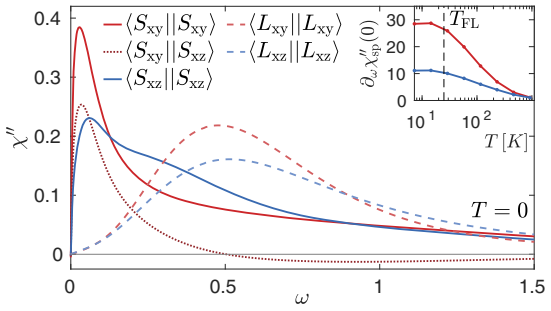


FIG. 2. Orbital-resolved, dynamic spin and angular-momentum susceptibilities, $\chi''(\omega)$. Inset: Temperature dependence of $\partial_\omega \chi''|_{\omega=0}$ in the spin sector, with $T_{FL}$ marked as a dashed line.

ground state, and total spin $S$. The most prominent tower of states stems from $xz/yz$ quasiparticles, i.e., eigenstates with quantum numbers (0,0,0), (0,1,1), (0,2,2), (0,2,0), (0,3,1), etc.; see solid lines in Fig. 1(b). States with an additional $xy$ quasiparticle are marked as dash-dotted lines. The Fermi-liquid scale $T_{FL}$ is seen in the RG flow as the point where eigenstates with equal charge but different spin become degenerate; see the pairs (0,2,0), (0,2,2) and (1,1,0), (1,1,2). Our direct evidence of the Fermi-liquid scale of $Sr_2RuO_4$, which conforms to the $T_{FL} \approx 25$ K found in experiments [21,28–31], is one of the main results of this work.

In order to understand how the different orbitals behave regarding spin-orbital scale separation, we investigate in Fig. 2 the orbitally resolved spin and angular-momentum susceptibilities [50]. We find strong orbital differentiation with larger amplitude in the $xy$ than the $xz$ spin response, and generally a shift of spectral weight to lower frequencies in the $xy$ compared to the $xz$ orbital. In nuclear magnetic resonance (NMR) spectroscopy, the inverse nuclear spin-lattice relaxation time, $1/(T_1T)$, is related to the zero-frequency slope of the electronic spin susceptibility, $1/(T_1T) \propto \partial_\omega \chi''|_{\omega=0}$ (neglecting matrix elements) [62,63]. Computing the orbitally resolved $\partial_\omega \chi''|_{\omega=0}$ as a function of temperature, we find that the $xy$ response is about 2.5 times stronger than the $xz$ response, see inset of Fig. 2, in qualitative agreement with experimental [31,64,65] and theoretical works [66]. The temperature dependence changes from linear to constant at $T_{FL}$, in a similar fashion for *both* orbitals, which we attribute to the strong orbital mixing on the two-particle level [39].

*Single-particle spectrum.*—Apart from the RG flow and (dynamic) susceptibilities, our calculations also provide single-particle spectral information. Although the single-particle properties of $Sr_2RuO_4$ have been studied extensively [24,26,27,33,38,45,48] using continuous-time quantum Monte Carlo (CTQMC) solvers [67], these calculations have a challenging scaling with inverse temperature $\beta$, making it hard to reach the Fermi-liquid regime with $T < 25$ K, i.e., $\beta > 464$ eV$^{-1}$. Additionally, the analytic continuation to real frequencies severely hampers spectral resolution [68]. Here, we go beyond previous works by analyzing $Sr_2RuO_4$ deep in the Fermi-liquid regime at low temperatures, and even $T = 0$, directly on the real-frequency axis.

The local spectral function $\mathcal{A}_{loc}(\omega)$ of $Sr_2RuO_4$ is considerably renormalized compared to the DFT DOS [24,45,48], see Fig. 3(a). When accounting for correlations, the spectral features are retained but shifted towards the Fermi level—both for the double peak in the $xz/yz$ orbitals and the narrow $xy$ peak. The latter is generated by the van Hove singularity in the $xy$ orbital, which is shifted towards the Fermi level by electronic correlations. The height of the van Hove peak grows with decreasing temperature and saturates below $T_{FL}$, see inset of Fig. 3(a).

The imaginary part of the self-energy $\mathrm{Im}\Sigma(\omega)$, shown in Fig. 3(b), determines the lifetime of excitations. It has larger values at negative compared to positive frequencies, yielding shorter lifetimes for hole excitations. Fermi-liquid behavior only emerges at frequencies below $T_{FL}$. The real part of the self-energy $\mathrm{Re}\Sigma(\omega)$ displays linear (Fermi-liquid) behavior on the same small energy scale, see

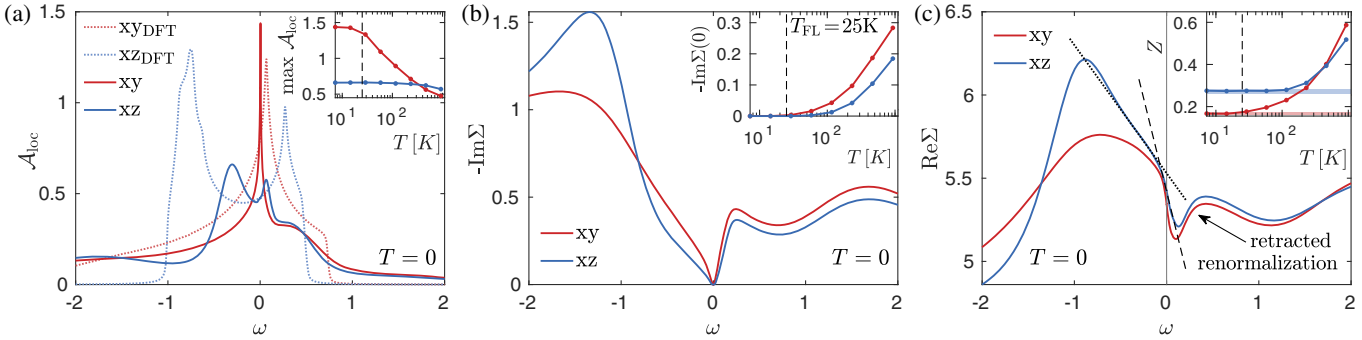


FIG. 3. Main panels: Real-frequency correlation functions at zero temperature. Insets: Characteristic values as a function of temperature, converging below $T_{FL}$ (dashed line). (a) Local spectral function, $\mathcal{A}_{loc}(\omega)$, from DFT + DMFT (solid lines) and DFT (dotted lines). Inset: $\max_\omega \mathcal{A}_{loc}(\omega)$. (b) Imaginary part of the self-energy, $\mathrm{Im}\Sigma(\omega)$. Inset: $\mathrm{Im}\Sigma(\omega = 0)$. (c) Real part of the self-energy, $\mathrm{Re}\Sigma(\omega)$, with the two linear regimes for $\omega < 0$ and the low-energy, positive slope for $\omega > 0$ highlighted. Inset: $Z = (1 - \partial_\omega \mathrm{Re}\Sigma|_{\omega=0})^{-1}$; thick horizontal lines show the $T = 0$ result for $Z$ calculated via renormalized parameters.

Fig. 3(c). However, at $\omega \approx -100$ meV, it exhibits a "kink" leading to a second linear regime [lines in Fig. 3(c)], while, for $\omega$ in the range $+200$–$400$ meV, the slope of $\mathrm{Re}\Sigma(\omega)$ changes sign, "retracting" the renormalization of the quasiparticle dispersion. Hence, in this energy range, the quasiparticle velocity is larger than the bare one [33], as opposed to the usual low-energy reduction due to strong correlations. These single-particle properties are in qualitative agreement with previous Monte Carlo results [24,26,27,33,38,45,48].

The pronounced differentiation between the different orbitals, seen in Figs. 1(b) and 2, is also reflected in the self-energy. The $xy$ orbital shows much stronger correlations than the $xz/yz$ ones, with higher curvature in $\mathrm{Im}\Sigma(\omega)$ and steeper slope in $\mathrm{Re}\Sigma(\omega)$ at $\omega = 0$, as visible in Figs. 3(b) and 3(c), respectively. The slope is related to the quasiparticle weight, $Z = (1 - \partial_\omega \mathrm{Re}\Sigma|_{\omega=0})^{-1}$, shown in the inset of Fig. 3(c). The zero-temperature values of $Z$ agree with renormalized parameters extracted directly from the spectrum (horizontal lines, see discussion below) and are also consistent with experiments [21,48]. The low-temperature relation $Z_{xy} < Z_{xz}$ contrasts with $Z_{xy} > Z_{xz}$ at high temperature. Indeed, when lowering temperature, the quasiparticle weights cross at $\sim$350 K, and, while $Z_{xz}$ levels off at $T \sim 100$ K, $Z_{xy}$ only saturates below $T_{\mathrm{FL}}$. This shows that the coherence-to-incoherence crossover and the corresponding coherence scales in $Sr_2RuO_4$ are strongly orbital dependent [24,40]. It is only below $T_{\mathrm{FL}}$ that *all* orbitals are in the coherent Fermi-liquid regime.

At first sight, the stronger correlation in the $xy$ orbital as compared to the $xz/yz$ orbitals, indicated by $Z_{xy} < Z_{xz}$, is rather counterintuitive. Usually, the ratio between the local Hubbard interaction $U$ and the bandwidth $W$, $U/W$, is a good estimator for the strength of correlations. However, this clearly does not hold for $Sr_2RuO_4$, since the $xy$ orbital has a significantly larger bandwidth, $W_{xy} > W_{xz}$, see Fig. 3(a). In Ref. [24], it has been argued that the strong $xy$ correlations result from the proximity of its van Hove singularity to the Fermi level, see Fig. 3(a).

To understand this, we consider the spectral part of the hybridization function $\mathcal{A}_\Delta(\omega)$ of the self-consistent impurity model. The van Hove singularity in $\mathcal{A}_{\mathrm{loc},xy}(\omega)$ generates a dip in $\mathcal{A}_{\Delta,xy}(\omega)$ [50] close to zero frequency, see Fig. 4(a), which implies a reduction of the effective coupling between impurity and bath at low energies for the $xy$ orbital. The weaker coupling, in turn, increases the correlations and reduces the quasiparticle weight. The temperature dependence of the dip, inset of Fig. 4(a), matches the one of $\max_\omega \mathcal{A}_{\mathrm{loc},xy}$ in the inset of Fig. 3(a).

To disentangle the effect of the van Hove singularity from other factors, we consider a simple, half-filled two-orbital model with both orbitals having the same bandwidth. We choose a semicircular lattice DOS for one orbital and set the second one such that its hybridization function has a dip at zero energy, see Fig. 4(b). Even in this simplified model, we find that $Z$ is smaller in the orbital with a dip in the hybridization. This suggests that the relevant measure of the correlation strength is the Hubbard interaction divided by the effective low-energy hybridization strength, $U/\mathcal{A}_\Delta(\omega = 0)$, rather than $U/W$.

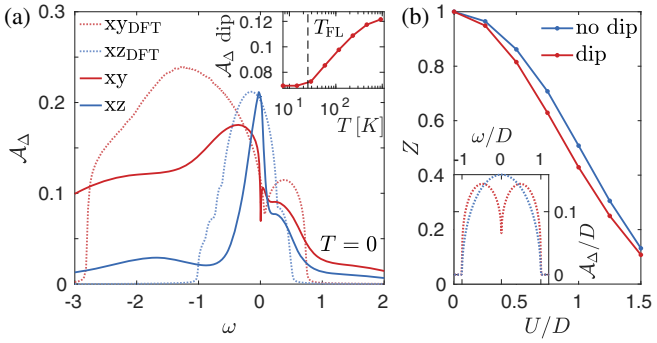


FIG. 4. (a) Spectral function of the hybridization $\mathcal{A}_\Delta(\omega)$ in DFT + DMFT (solid lines) and DFT (dotted lines). Inset: temperature dependence of the van Hove dip in $\mathcal{A}_{\Delta,xy}(\omega)$. (b) Quasiparticle weight $Z$ as a function of Hubbard $U$, for a simple two-orbital model with identical half bandwidth $D$. The hybridization functions at $U = 0$ are shown in the inset.

*Quasiparticle parameters.*—Within the NRG framework, we can extract information about the Fermi liquid and its quasiparticles not only from correlation functions but directly from the RG flow. To this end, we compute (zero-temperature) renormalized parameters from the low-energy spectrum of the (self-consistent) impurity model [69–72]. The impurity Green's function has the low-energy expansion

$$G(\omega) \approx Z[\omega - \tilde{\epsilon} - Z\Delta(\omega)]^{-1}, \qquad \tilde{\epsilon} = Z[\epsilon + \Sigma(0)].$$

For a (finite) Wilson chain of length $N$, $G(\omega)$ has first-order poles at the single-particle excitation energies. Taking the lowest particle- and hole-excitation energy $E_i(N)$ from Fig. 1(b), we have two equations that can be solved for $Z$ and $\tilde{\epsilon}$ and converged in $N$ [69]. The results for $Z$ [and $\tilde{\epsilon}$ or $\Sigma(0)$] are reported in Ref. [50] and agree quantitatively with those taken from $\Sigma(\omega)$, see inset of Fig. 3(c).

To go beyond the single-particle picture, we exploit that, at any finite $N$, there are residual quasiparticle interactions in the form of exponentially small corrections to the equidistant tower of quasiparticle excitations. By comparing two-particle-excitation energies $E^S_{mm'}$, with orbital indices $m$ and $m'$ and spin index $S$, to two single-particle excitations $E_m$ and $E_{m'}$, the quasiparticle interaction $\tilde{U}^S_{mm'}$ is given by [69]

$$E^S_{mm'} - E_m - E_{m'} = \tilde{U}^S_{mm'} |\psi_m(0)|^2 |\psi_{m'}(0)|^2,$$

where $|\psi_m(0)|^2$ is the quasiparticle density at the impurity [50]. Hence, we are in the unique position to compute quasiparticle interactions $\tilde{U}^S_{mm'}$ as well as the zero-energy

real-frequency vertex $\Gamma$, related via $\tilde{U}^S_{mm'} = Z_m Z_{m'} \Gamma^S_{mm'}$ [69,71], for $Sr_2RuO_4$. The results, listed in Ref. [50], show that the orbital dependence of $\tilde{U}^S_{mm'}$ is governed by $Z_m$, while $\Gamma^S_{mm'}$ displays only weak orbital dependence. Strikingly, the effective interaction in the spin-triplet sector is *attractive*. We attribute this to the same mechanism as the Hund-metal *s*-wave spin-triplet superconducting instability found in model studies [74,75].

*Conclusion.*—By following the NRG flow starting from high and proceeding to the lowest temperature and energy scales, we have analyzed spin-orbital scale separation and the emergence of the Fermi liquid in $Sr_2RuO_4$ within a real-materials DFT + DMFT setting. Through linear frequency behavior of zero-temperature dynamic susceptibilities and fixed-point analysis of the NRG flow, we provide theoretical evidence for a Fermi-liquid scale, in remarkable agreement with the experimentally observed $T_{\mathrm{FL}} \approx 25$ K [21,28–31]. Characteristic quantities, like $\chi_{\mathrm{sp}}$ and $Z$, are found to converge below 25 K. Further, our real-frequency and zero-temperature results substantiate a number of features, such as strongly shifted spectral peaks and the peculiar frequency dependence of the self-energy, previously found from analytically continued Monte Carlo data [24,26,27,33,38–41]. We showed that the proximity of the van Hove singularity to the Fermi level drives strong orbital differentiation in $Sr_2RuO_4$. Notably, the effect of van Hove singularities on the correlated state is of importance even in nontransition metal systems like twisted bilayer graphene [76–78]. Finally, the extracted quasiparticle interactions $\tilde{U}^S_{mm'}$ reveal attractive coupling in the spin-triplet sector within our *ab initio* analysis. This paves the way towards a complete description of quasiparticles and their interactions in $Sr_2RuO_4$, which are of crucial importance for the understanding of the still puzzling superconducting state [23,79].

Generally, our work demonstrates the potential of DFT + DMFT + NRG as a new computational paradigm for real-material systems to (i) directly access real-frequency properties at arbitrarily low temperatures and (ii) reveal and elucidate the intricate renormalization process that occurs during the dressing of atomic excitations by their solid-state environment.

We thank G. Kotliar, J. Mravlje, and A. Weichselbaum for fruitful discussions. The NRG results were obtained using the QSpace tensor library [80,81], and TRIQS applications [82–84] were used; see Ref. [50] for details. F. B. K., S.-S. B. L., and J. v. D. are supported by the Deutsche Forschungsgemeinschaft under Germany's Excellence Strategy—EXC-2111–390814868; S.-S. B. L. further by Grant No. LE3883/2-1. F. B. K. acknowledges funding from the research school IMPRS-QST and is grateful for hospitality at the Flatiron Institute, where most of this work was carried out. The Flatiron Institute is a division of the Simons Foundation.

[1] S. Sugano, Y. Tanabe, and H. Kamimura, *Multiplets of Transition-Metal Ions in Crystals* (Academic Press Inc., New York, 1970), http://www.sciencedirect.com/bookseries/pure-and-applied-physics/vol/33.
[2] A. Georges, L. de' Medici, and J. Mravlje, Annu. Rev. Condens. Matter Phys. **4**, 137 (2013).
[3] M. Imada, A. Fujimori, and Y. Tokura, Rev. Mod. Phys. **70**, 1039 (1998).
[4] A. Georges, G. Kotliar, W. Krauth, and M. J. Rozenberg, Rev. Mod. Phys. **68**, 13 (1996).
[5] J. Kondo, Prog. Theor. Phys. **32**, 37 (1964).
[6] K. M. Stadler, Z. P. Yin, J. von Delft, G. Kotliar, and A. Weichselbaum, Phys. Rev. Lett. **115**, 136401 (2015).
[7] X. Deng, K. M. Stadler, K. Haule, A. Weichselbaum, J. von Delft, and G. Kotliar, Nat. Commun. **10**, 2721 (2019).
[8] K. G. Wilson, Rev. Mod. Phys. **47**, 773 (1975).
[9] R. Bulla, T. A. Costi, and T. Pruschke, Rev. Mod. Phys. **80**, 395 (2008).
[10] T. Pruschke and R. Bulla, Eur. Phys. J. B **44**, 217 (2005).
[11] R. Peters and T. Pruschke, Phys. Rev. B **81**, 035112 (2010).
[12] R. Peters and T. Pruschke, J. Phys. Conf. Ser. **200**, 012158 (2010).
[13] R. Peters, N. Kawakami, and T. Pruschke, Phys. Rev. B **83**, 125110 (2011).
[14] M. Greger, M. Kollar, and D. Vollhardt, Phys. Rev. Lett. **110**, 046403 (2013).
[15] M. Greger, M. Sekania, and M. Kollar, arXiv:1312.0100.
[16] A. Horvat, R. Žitko, and J. Mravlje, Phys. Rev. B **94**, 165140 (2016).
[17] A. Horvat, R. Žitko, and J. Mravlje, Phys. Rev. B **96**, 085122 (2017).
[18] K. Stadler, G. Kotliar, A. Weichselbaum, and J. von Delft, Ann. Phys. (Amsterdam) **405**, 365 (2019).
[19] F. B. Kugler, S.-S. B. Lee, A. Weichselbaum, G. Kotliar, and J. von Delft, Phys. Rev. B **100**, 115159 (2019).
[20] G. Kotliar, S. Y. Savrasov, K. Haule, V. S. Oudovenko, O. Parcollet, and C. A. Marianetti, Rev. Mod. Phys. **78**, 865 (2006).
[21] A. P. Mackenzie and Y. Maeno, Rev. Mod. Phys. **75**, 657 (2003).
[22] Y. Maeno, H. Hashimoto, K. Yoshida, S. Nishizaki, T. Fujita, J. G. Bednorz, and F. Lichtenberg, Nature (London) **372**, 532 (1994).
[23] A. P. Mackenzie, T. Scaffidi, C. W. Hicks, and Y. Maeno, Quantum Mater. **2**, 40 (2017).
[24] J. Mravlje, M. Aichhorn, T. Miyake, K. Haule, G. Kotliar, and A. Georges, Phys. Rev. Lett. **106**, 096401 (2011).
[25] L. de' Medici, J. Mravlje, and A. Georges, Phys. Rev. Lett. **107**, 256401 (2011).
[26] J. Mravlje and A. Georges, Phys. Rev. Lett. **117**, 036401 (2016).
[27] M. Kim, J. Mravlje, M. Ferrero, O. Parcollet, and A. Georges, Phys. Rev. Lett. **120**, 126401 (2018).
[28] N. E. Hussey, A. P. Mackenzie, J. R. Cooper, Y. Maeno, S. Nishizaki, and T. Fujita, Phys. Rev. B **57**, 5505 (1998).
[29] T. Katsufuji, M. Kasai, and Y. Tokura, Phys. Rev. Lett. **76**, 126 (1996).
[30] Y. Maeno, K. Yoshida, H. Hashimoto, S. Nishizaki, S.-I. Ikeda, M. Nohara, T. Fujita, A. P. Mackenzie, N. E. Hussey, J. G. Bednorz, and F. Lichtenberg, J. Phys. Soc. Jpn. **66**, 1405 (1997).

[31] T. Imai, A. W. Hunt, K. R. Thurber, and F. C. Chou, Phys. Rev. Lett. **81**, 3006 (1998).

[32] A. Mackenzie, S. Julian, A. Diver, G. Lonzarich, N. Hussey, Y. Maeno, S. Nishizaki, and T. Fujita, Physica (Amsterdam) **263C**, 510 (1996).

[33] D. Stricker, J. Mravlje, C. Berthod, R. Fittipaldi, A. Vecchione, A. Georges, and D. van der Marel, Phys. Rev. Lett. **113**, 087404 (2014).

[34] The orbital and spin Kondo temperatures, $T_{\mathrm{orb}}$ and $T_{\mathrm{sp}}$, give the characteristic energy scale of the corresponding screening process and are here deduced from the maxima of the respective zero-temperature real-frequency susceptibilities [6,18,19]. Similarly, the Fermi-liquid crossover, which corresponds to the *completion* of the screening process [7], is associated with a scale as opposed to an exact number. In this case, we do not extract a specific value but rather compare the experimentally observed 25 K [21,28–31] to our numerical data and demonstrate excellent agreement.

[35] We note that also tensor networks have been successfully used to carry out DFT + DMFT calculations directly on the real-frequency axis [36,37].

[36] D. Bauernfeind, M. Zingl, R. Triebl, M. Aichhorn, and H. G. Evertz, Phys. Rev. X **7**, 031013 (2017).

[37] D. Bauernfeind, R. Triebl, M. Zingl, M. Aichhorn, and H. G. Evertz, Phys. Rev. B **97**, 115156 (2018).

[38] G. Zhang, E. Gorelov, E. Sarvestani, and E. Pavarini, Phys. Rev. Lett. **116**, 106402 (2016).

[39] H. U. R. Strand, M. Zingl, N. Wentzell, O. Parcollet, and A. Georges, Phys. Rev. B **100**, 125120 (2019).

[40] M. Zingl, J. Mravlje, M. Aichhorn, O. Parcollet, and A. Georges, Quantum Mater. **4**, 35 (2019).

[41] X. Deng, K. Haule, and G. Kotliar, Phys. Rev. Lett. **116**, 256401 (2016).

[42] Currently, also a matrix product states (MPS) based impurity solver is being used to study $Sr_2RuO_4$ at $T = 0$, although on the Matsubara axis [43].

[43] N.-O. Linden, M. Zingl, C. Hubig, O. Parcollet, and U. Schollwöck, arXiv:1909.02503.

[44] C. Bergemann, A. P. Mackenzie, S. R. Julian, D. Forsythe, and E. Ohmichi, Adv. Phys. **52**, 639 (2003).

[45] E. Sarvestani, G. Zhang, E. Gorelov, and E. Pavarini, Phys. Rev. B **97**, 085141 (2018).

[46] N. Marzari and D. Vanderbilt, Phys. Rev. B **56**, 12847 (1997).

[47] I. Souza, N. Marzari, and D. Vanderbilt, Phys. Rev. B **65**, 035109 (2001).

[48] A. Tamai *et al.*, Phys. Rev. X **9**, 021048 (2019).

[49] J. Kanamori, Prog. Theor. Phys. **30**, 275 (1963).

[50] See Supplemental Material at http://link.aps.org/supplemental/10.1103/PhysRevLett.124.016401 for further definitions, algorithmic details, and the quasiparticle parameters, which additionally contains Refs. [51–61] listed below.

[51] P. Werner, A. Comanac, L. de' Medici, M. Troyer, and A. J. Millis, Phys. Rev. Lett. **97**, 076405 (2006).

[52] P. Blaha, K. Schwarz, G. K. H. Madsen, D. Kvasnicka, J. Luitz, R. Laskowski, F. Tran, and L. D. Marks, *WIEN2k, An Augmented Plane Wave+Local Orbitals Program for Calculating Crystal Properties* (K. Schwarz, Techn. Univ. Wien, Austria, 2018).

[53] K. Kuneš, R. Arita, P. Wissgott, A. Toschi, H. Ikeda, and K. Held, Comput. Phys. Commun. **181**, 1888 (2010).

[54] A. A. Mostofi, J. R. Yates, G. Pizzi, Y.-S. Lee, I. Souza, D. Vanderbilt, and N. Marzari, Comput. Phys. Commun. **185**, 2309 (2014).

[55] A. Weichselbaum and J. von Delft, Phys. Rev. Lett. **99**, 076402 (2007).

[56] A. K. Mitchell, M. R. Galpin, S. Wilson-Fletcher, D. E. Logan, and R. Bulla, Phys. Rev. B **89**, 121105(R) (2014).

[57] K. M. Stadler, A. K. Mitchell, J. von Delft, and A. Weichselbaum, Phys. Rev. B **93**, 235101 (2016).

[58] R. Žitko and T. Pruschke, Phys. Rev. B **79**, 085106 (2009).

[59] S.-S. B. Lee and A. Weichselbaum, Phys. Rev. B **94**, 235127 (2016).

[60] S.-S. B. Lee, J. von Delft, and A. Weichselbaum, Phys. Rev. Lett. **119**, 236402 (2017).

[61] H. U. R. Strand, https://dx.doi.org/10.5281/zenodo.2638059, 2019.

[62] H. Alloul, Scholarpedia **9**, 32069 (2014).

[63] H. Alloul, Scholarpedia **10**, 30632 (2015).

[64] H. Mukuda, K. Ishida, Y. Kitaoka, K. Asayama, Z. Mao, Y. Mori, and Y. Maeno, J. Phys. Soc. Jpn. **67**, 3945 (1998).

[65] K. Ishida, H. Mukuda, Y. Minami, Y. Kitaoka, Z. Q. Mao, H. Fukazawa, and Y. Maeno, Phys. Rev. B **64**, 100501(R) (2001).

[66] J. Mravlje, M. Aichhorn, T. Miyake, K. Haule, G. Kotliar, and A. Georges, Phys. Rev. Lett. **106**, 096401 (2011).

[67] E. Gull, A. J. Millis, A. I. Lichtenstein, A. N. Rubtsov, M. Troyer, and P. Werner, Rev. Mod. Phys. **83**, 349 (2011).

[68] J. E. Gubernatis, M. Jarrell, R. N. Silver, and D. S. Sivia, Phys. Rev. B **44**, 6011 (1991).

[69] A. C. Hewson, A. Oguri, and D. Meyer, Eur. Phys. J. B **40**, 177 (2004).

[70] J. Bauer and A. C. Hewson, Phys. Rev. B **76**, 035118 (2007).

[71] Y. Nishikawa, D. J. G. Crow, and A. C. Hewson, Phys. Rev. B **82**, 115123 (2010).

[72] See Ref. [73] for the relation between the Landau parameters of the lattice and the (self-consistent) impurity model.

[73] F. Krien, E. G. C. P. van Loon, M. I. Katsnelson, A. I. Lichtenstein, and M. Capone, Phys. Rev. B **99**, 245128 (2019).

[74] S. Hoshino and P. Werner, Phys. Rev. Lett. **115**, 247001 (2015).

[75] S. Hoshino and P. Werner, Phys. Rev. B **93**, 155161 (2016).

[76] G. Li, A. Luican, J. M. B. L. dos Santos, A. H. C. Neto, A. Reina, J. Kong, and E. Y. Andrei, Nat. Phys. **6**, 109 (2010).

[77] A. Kerelsky, L. J. McGilly, D. M. Kennes, L. Xian, M. Yankowitz, S. Chen, K. Watanabe, T. Taniguchi, J. Hone, C. Dean, A. Rubio, and A. N. Pasupathy, Nature (London) **572**, 95 (2019).

[78] Y. Choi, J. Kemmer, Y. Peng, A. Thomson, H. Arora, R. Polski, Y. Zhang, H. Ren, J. Alicea, G. Refael, F. von Oppen, K. Watanabe, T. Taniguchi, and S. Nadj-Perge, Nat. Phys. **15**, 1174 (2019).

[79] A. Pustogow, Y. Luo, A. Chronister, Y. S. Su, D. A. Sokolov, F. Jerzembeck, A. P. Mackenzie, C. W. Hicks, N. Kikugawa, S. Raghu, E. D. Bauer, and S. E. Brown, Nature (London) **574**, 72 (2019).

[80] A. Weichselbaum, Ann. Phys. (Amsterdam) **327**, 2972 (2012).
[81] A. Weichselbaum, Phys. Rev. B **86**, 245124 (2012).
[82] O. Parcollet, M. Ferrero, T. Ayral, H. Hafermann, I. Krivenko, L. Messio, and P. Seth, Comput. Phys. Commun. **196**, 398 (2015).
[83] P. Seth, I. Krivenko, M. Ferrero, and O. Parcollet, Comput. Phys. Commun. **200**, 274 (2016).
[84] M. Aichhorn, L. Pourovskii, P. Seth, V. Vildosola, M. Zingl, O. E. Peil, X. Deng, J. Mravlje, G. J. Kraberger, C. Martins, M. Ferrero, and O. Parcollet, Comput. Phys. Commun. **204**, 200 (2016).